Real-time quadrature projection complex conjugate resolved Fourier domain optical coherence tomography

Marinko V. Sarunic, Brian E. Applegate, and Joseph A. Izatt

Department of Biomedical Engineering, Duke University, Durham, North Carolina 27708

Received February 16, 2006; revised April 30, 2006; accepted May 9, 2006;
posted June 1, 2006 (Doc. ID 68196); published July 25, 2006

We present a novel algorithm for full-range imaging by suppression of the complex conjugate artifact in phase-shifting Fourier domain optical coherence tomography. This technique utilizes the projection of multiple phase-shifted interferograms onto an orthogonal basis set to reconstruct the complex interferogram. Full-range imaging with >30 dB suppression of the symmetric artifact is demonstrated using a 3×3 fiber coupler swept source OCT system, providing a depth range of 6.6 mm with −8 dB roll-off in sensitivity at the depth boundaries relative to DC. Real-time display of full-range images of the anterior segment of the human eye acquired *in vivo* at a line rate of 6.67 kHz are presented. © 2006 Optical Society of America

OCIS codes: 110.4500, 120.5050, 120.3890.

Development of optical coherence tomography[1] (OCT) in recent years has concentrated on Fourier domain (FD) techniques[2] for high-speed cross-sectional imaging of biological tissue. In FDOCT, the locations of scatterers within a sample are obtained by Fourier transformation of real-valued spectral interferograms. The Fourier transform of the interferogram is Hermitian symmetric, introducing a complex conjugate artifact in which positive and negative distances are not resolved. In practice, this artifact may be avoided by locating the sample entirely within the positive or negative displacement range, thus utilizing only half the total imaging depth. Such one-sided imaging is suitable for thin objects, but imaging of extended objects is limited by the characteristic sensitivity roll-off due to the finite spectral resolution of FDOCT systems.[3]

Full-range imaging, in which positive and negative distances are resolved, can be achieved by indirectly measuring the complex component of the interferometric OCT signal obtained by shifting the phase of the reference reflection in increments of 90°.[4–7] Sequentially shifting the reference reflector phase has been demonstrated in spectrometer-based FDOCT[4–6] but suffered from significant image corruption resulting from small (including chromatic) deviations in the actual phase shift or from small (subwavelength) sample motion between the phase-shifted acquisitions. Recently, the instantaneous acquisition of two phase-shifted signals was demonstrated using linearly polarized light.[8] Complex signal reconstruction was limited by having only two phase-shifted signals and also by potential image corruption in birefringent samples. We have previously described methods to instantaneously acquire three phase-shifted interferograms using 3×3 fused fiber couplers for both spectrometer-based and swept source (SS) FDOCT systems.[7] The performance of these systems was limited by the wavelength dependence of the splitting ratios of the couplers. A frequency-shifting approach to full-range imaging has also been presented in the literature[9] but is not compatible with spectrometer-based systems.

All the phase-shifting FDOCT techniques described thus far suffer image corruption arising from miscalibration of the phase shifts and also from the wavelength dependence of the phase shifter. A least squares fitting algorithm has been presented in the literature to improve the suppression of symmetric artifacts by correcting for phase-shift irregularities and also by accounting for axial sample motion in between phase-shifted acquisitions.[6] In this Letter, we present a novel algorithm for complex conjugate resolved FDOCT imaging by projecting phase-shifted signals onto an orthogonal basis set using Fourier decomposition. Quadrature projection processing is insensitive to miscalibrated phase shifts in 90° shift interferometry and requires only predetermination of the quadrant location for each phase shift in non-90° techniques.

The interferometric component of the detector signal in a phase-shifting FDOCT system can be written as $s_n(k) \propto \Sigma A_m \cos(2\Delta z_m k + \theta_m + \phi_n)$, where Δz_m, A_m, and θ_m represent the axial distance, the reflectance, and the relative phase of the mth scatterer in the sample, respectively, and ϕ_n is an additional phase shift introduced for the nth phase-shifted acquisition. Three representative interferograms, $s_n(k)$, phase shifted by nominally 120° are shown in Fig. 1a. Since the interferograms differ only by an external phase shift (corresponding to less than a wavelength), the Fourier transform of each signal, $\hat{s}_n(z) = \mathrm{FT}\{s_n(k)\}$, has the same intensity depth profile, but the phase at each corresponding depth differs by the induced phase shift, ϕ_n. The Fourier transformed signals, $\hat{s}_n(z)$, can be represented vectorally in the complex plane by plotting the depth-resolved magnitude $\|\hat{s}_n(z_m)\|$ at an angle $\theta_m + \phi_n$, as illustrated in Fig. 1b (showing only a single reflector for clarity), with the possible values of θ_m ranging from 0 to 2π.

The first step of quadrature projection processing

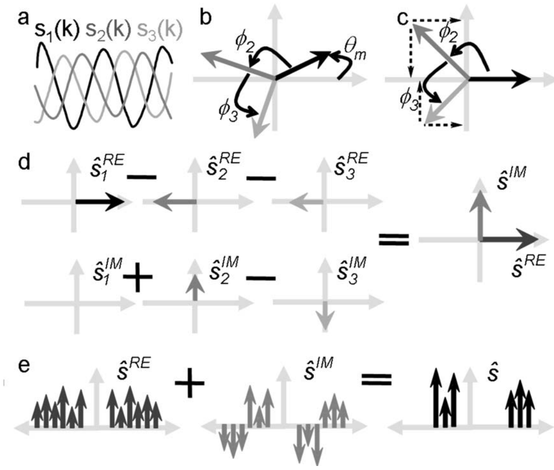

Fig. 1. Quadrature projection processing steps. The phase-shifted interferograms shown in a are Fourier transformed, and each depth location can be represented in the complex plane, b. Phase subtraction aligns the first signal onto the positive real axis, and the shifted signals are forced to the angle of the induced phase shift, c. The projections of each vector onto the real and imaginary axis are summed, accounting for the sign of each component, d. The complex conjugate resolved signal is obtained by adding the symmetric real and antisymmetric imaginary components, e.

is to remove the depth dependence of the phase, θ_m, to align the phase at all depths with the induced phase shift ϕ_n. This is accomplished by subtracting the phase profile of the first signal from each of the phase-shifted signals; $\hat{s}_n'(z)=\|\hat{s}_n(z)\|\exp\{\arg[\hat{s}_n(z)]-\arg[\hat{s}_1(z)]\}$. The result of the phase subtraction is illustrated vectorally in Fig. 1c for a single reflector and shows that $\hat{s}_1'(z)$ is aligned with the positive real axis while the remaining phase-shifted signals are forced onto the angle induced by the phase shift, ϕ_n. This phase subtraction introduces an axial shift of each scatterer by up to $\lambda/2$, which is much smaller than the coherence length for practical light sources used in OCT. Note that the phase is referenced relative to the first detector signal and does not require knowledge of ϕ_n.

The second step in the algorithm is to calculate the quadrature components of each phase referenced signal $\hat{s}_n'(z)$. As illustrated in Fig. 1c by the dashed arrows, this step is analogous to calculating the projection of each vector onto the real and imaginary axes. This is performed using Fourier decomposition by simply expressing the complex-valued $\hat{s}_n'(z)$ in rectangular coordinates and taking the real and imaginary parts, $\hat{s}_n^{\mathrm{RE}}(z)=\mathrm{Re}\{\hat{s}_n'(z)\}$ and $\hat{s}_n^{\mathrm{IM}}(z)=\mathrm{Im}\{\hat{s}_n'(z)\}$. The derived $\hat{s}_n^{\mathrm{RE}}(z)$ and $\hat{s}_n^{\mathrm{IM}}(z)$ are in quadrature irrespective of the induced phase shift ϕ_n because the cosine and sine basis functions are orthogonal. Dependence of ϕ_n on wavenumber does not affect the orthogonality of the projections. Note that both $\hat{s}_n^{\mathrm{RE}}(z)$ and $\hat{s}_n^{\mathrm{IM}}(z)$ are real valued and that the depth profile of $\hat{s}_n^{\mathrm{RE}}(z)$ is symmetric, whereas $\hat{s}_n^{\mathrm{IM}}(z)$ is antisymmetric.

The next step in the quadrature projection algorithm is to combine the quadrature components of the phase-shifted signals. When utilized in conjunction with 90° phase-shifting techniques, only the projection along the desired axis is retained. A nonzero value of the perpendicular component represents a miscalibrated phase shift and/or sample drift. When quadrature projection is used with non-90° phase-shifting techniques, the real and imaginary components are of similar amplitude and both are retained. An estimate of each ϕ_n is required to predetermine which quadrature-projected components are aligned parallel or antiparallel to the axes, represented using $\delta_n^{\mathrm{RE}}=\pm 1$ and $\delta_n^{\mathrm{IM}}=\pm 1$. Since the sign of each δ_n is dependent only on the quadrant location of ϕ_n, the quadrature-projection algorithm is insensitive to miscalibration or drift of the actual induced phase shift. The derived real and imaginary signals are thus determined using the relations $\hat{s}^{\mathrm{RE}}(z)=\Sigma_n \delta_n^{\mathrm{RE}}\hat{s}_n^{\mathrm{RE}}$ and $\hat{s}^{\mathrm{IM}}(z)=\Sigma_n \delta_n^{\mathrm{IM}}\hat{s}_n^{\mathrm{IM}}$, illustrated in Fig. 1d.

Lastly, the derived quadrature components $\hat{s}^{\mathrm{RE}}(z)$ and $\hat{s}^{\mathrm{IM}}(z)$ require scaling to account for unequal contributions to the real and imaginary quadrature components. The scaling coefficient is calculated using β, the ratio of the total energy in the derived real signal to that of the derived imaginary signal, given by $\beta=[\int|\hat{s}^{\mathrm{RE}}(z)|^2 dz/\int|\hat{s}^{\mathrm{IM}}(z)|^2 dz]^{1/2}$. The complex conjugate resolved A-scan is then obtained by directly adding the derived real component and the scaled imaginary component, $\hat{s}(z)=\hat{s}^{\mathrm{RE}}(z)+\beta\cdot\hat{s}^{\mathrm{IM}}(z)$. The summation is illustrated in Fig. 1d, showing cancellation of the symmetric complex conjugate artifact peaks in $\hat{s}^{\mathrm{RE}}(z)$ by the antisymmetric peaks in $\hat{s}^{\mathrm{IM}}(z)$, resulting in the full-range depth profile $\hat{s}(z)$.

Quadrature projection processing was demonstrated using the 3×3 Michelson-type interferometer illustrated in Fig. 2. The source was a fiber ring swept laser (Micron Optics) followed by a semiconductor optical amplifier (InPhenix),[10] providing a FWHM bandwidth of 84 nm centered at 1310 nm, and an average power of >8 mW at the sample. The source was driven with a 3.33 kHz triangular wave, providing an effective 6.67 kHz line rate by processing both forward and backward sweeps. A calibration signal from a 2×2 fiber Michelson interferometer was used to resample the data channels using the nearest-neighbor algorithm presented by Huber *et al.*[10] All four channels were digitized simultaneously at 10 MHz (NI PCI 6115), from four photodiode detectors (New Focus $D_{1\text{-}3}$, Model 1817, and D_4, Model 1617).

The optical power at the sample was reduced to 3.75 mW for ocular anterior segment imaging, and

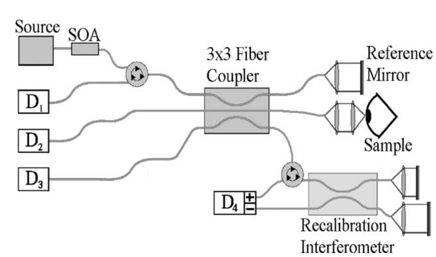

Fig. 2. SS OCT system using a 3×3 fused fiber coupler in a Michelson-type interferometer.

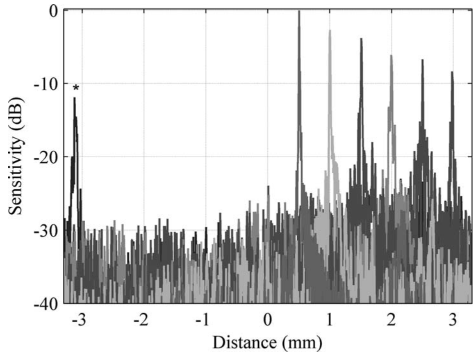

Fig. 3. Complex conjugate resolved A-scans with a −50 dB attenuated sample reflector demonstrating a sensitivity of 103 dB with a roll-off of −8 dB at 3.3 mm and >30 dB suppression of the complex conjugate artifact. The asterisk represents an aliased positive path length difference of 3.5 mm, which appears as a negative distance.

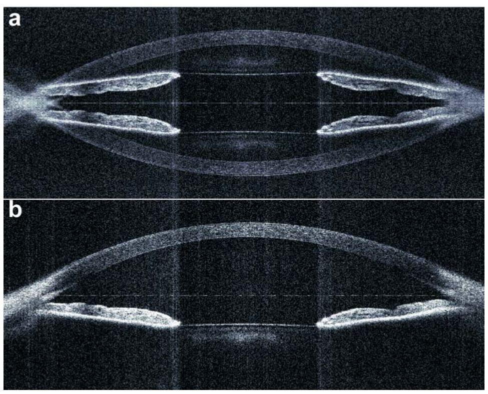

Fig. 4. *In vivo* full-depth images of the ocular anterior segment in a human volunteer. The image in a is corrupted by the complex conjugate artifact. Applying the quadrature projection algorithm uniquely resolves positive and negative distances as shown in b. Each image consists of 800 vertical lines with 1024 samples per line.

this value was also used to measure the system sensitivity. The complex conjugate suppression of >30 dB and resulting double-sided imaging depth of 6.6 mm are presented in Fig. 3. The system sensitivity, accounting for recoupling losses, was measured to be 103 dB near DC and decreased by 8 dB at the ends of the depth scan. The quadrature projection 3×3 SS OCT system was demonstrated for *in vivo* imaging of the ocular anterior segment of human volunteers with approval from the Institutional Review Board of Duke University Medical Center. Corruption of the complex conjugate resolved image due to sample motion was not observed since the phase-shifted interferograms from the 3×3 coupler were acquired simultaneously. Custom C++ code was written for efficient image processing on a standard desktop (Intel Pentium D 3.2 GHz) computer. The nearest-neighbor resampling[10] and quadrature projection processing were performed and displayed in real time on 1024 point A-scans for 800 lines per frame at 6.7 frames/s. The complex conjugate resolved image is compared against the unresolved image (obtained by averaging the Fourier transformed detector outputs) in Fig. 4.

In conclusion, we have presented a novel algorithm for complex conjugate resolved FDOCT with arbitrarily spaced phase shifts. The algorithm was demonstrated using a 3×3 fiber interferometer but is generally applicable to other phase-shifting techniques.

Funding for this research was provided by National Institutes of Health grant EY013516, and B. E. Applegate acknowledges support via National Institutes of Health postdoctoral fellowship EB004237. We thank Bioptigen, Inc., for the base acquisition software, Kevin Hsu of Micron Optics, Inc., for loan of the swept source laser module, and Robert Zawadzki for insightful discussions. M. Sarunic's e-mail address is marinko.sarunic@duke.edu.

References

1. D. Huang, E. A. Swanson, C. P. Lin, J. S. Schuman, W. G. Stinson, W. Chang, M. R. Hee, T. Flotte, K. Gregory, C. A. Puliafito, and J. G. Fujimoto, Science **254**, 1178 (1991).
2. F. Fercher, C. K. Hitzenberger, G. Kamp, and S. Y. Elzaiat, Opt. Commun. **117**, 43 (1995).
3. C. Dorrer, N. Belabas, J. P. Likforman, and M. Joffre, J. Opt. Soc. Am. B **17**, 1795 (2000).
4. M. Wojtkowski, A. Kowalczyk, R. Leitgeb, and A. F. Fercher, Opt. Lett. **27**, 1415 (2002).
5. E. Gotzinger, M. Pircher, R. A. Leitgeb, and C. K. Hitzenberger, Opt. Express **13**, 583 (2005).
6. P. Targowski, W. Gorczynska, M. Szkulmowski, M. Wojtkowski, and A. Kowalczyk, Opt. Commun. **249**, 357 (2005).
7. M. V. Sarunic, M. A. Choma, C. Yang, and J. A. Izatt, Opt. Express **13**, 957 (2005).
8. B. J. Vakoc, S. H. Yun, G. J. Tearney, and B. E. Bouma, Opt. Lett. **31**, 362 (2006).
9. S. H. Yun, G. J. Tearney, J. F. De Boer, and B. E. Bouma, Opt. Express **12**, 4822 (2004).
10. R. Huber, M. Wojtkowski, K. Taira, J. G. Fujimoto, and K. Hsu, Opt. Express **13**, 3513 (2005).